LETTER

https://doi.org/10.1038/s41586-019-1375-0

Giant thermal Hall conductivity in the pseudogap phase of cuprate superconductors

G. Grissonnanche[1]*, A. Legros[1,2], S. Badoux[1], E. Lefrançois[1], V. Zatko[1], M. Lizaire[1], F. Laliberté[1], A. Gourgout[1], J.-S. Zhou[3], S. Pyon[4,5], T. Takayama[4,6], H. Takagi[4,6,7,8], S. Ono[9], N. Doiron-Leyraud[1] & L. Taillefer[1,10]*

The nature of the pseudogap phase of the copper oxides ('cuprates') remains a puzzle. Although there are indications that this phase breaks various symmetries, there is no consensus on its fundamental nature[1]. Fermi-surface, transport and thermodynamic signatures of the pseudogap phase are reminiscent of a transition into a phase with antiferromagnetic order, but evidence for an associated long-range magnetic order is still lacking[2]. Here we report measurements of the thermal Hall conductivity (in the x–y plane, κ_{xy}) in the normal state of four different cuprates—$La_{1.6-x}Nd_{0.4}Sr_xCuO_4$, $La_{1.8-x}Eu_{0.2}Sr_xCuO_4$, $La_{2-x}Sr_xCuO_4$ and $Bi_2Sr_{2-x}La_xCuO_{6+\delta}$. We show that a large negative κ_{xy} signal is a property of the pseudogap phase, appearing at its critical hole doping, p^*. It is also a property of the Mott insulator at $p \approx 0$, where κ_{xy} has the largest reported magnitude of any insulator so far[3]. Because this negative κ_{xy} signal grows as the system becomes increasingly insulating electrically, it cannot be attributed to conventional mobile charge carriers. Nor is it due to magnons, because it exists in the absence of magnetic order. Our observation is reminiscent of the thermal Hall conductivity of insulators with spin-liquid states[4–6], pointing to neutral excitations with spin chirality[7] in the pseudogap phase of cuprates.

Among the different families of unconventional superconductors, magnetism and superconductivity are often closely associated[8]. A notable exception is the family of hole-doped cuprates, where superconductivity mostly coexists instead with the pseudogap phase, which is an enigmatic state of matter whose nature remains unclear[1]. The critical doping p^* (for the onset of the pseudogap phase) bears the hallmarks of an antiferromagnetic quantum critical point[2], with a sharp drop in the carrier density n from $n \approx 1 + p$ above p^* to $n \approx p$ below p^*, a resistivity linear with temperature T, and a specific heat with a $\log(1/T)$ dependence. Yet, there is no evidence for long-range magnetic order appearing at p^*. However, numerical solutions of the Hubbard model have shown that a pseudogap phase can arise from short-range antiferromagnetic correlations[9]. It has been argued that an exotic state with topological order can account for such a pseudogap and for the drop in carrier density without breaking translational symmetry[10], but the low-energy excitations of such a state have yet to be detected.

In recent years, the thermal Hall effect has emerged as a powerful probe of magnetic texture and topological excitations in insulators. On the theory side, a non-zero thermal Hall conductivity κ_{xy} was shown to arise even without long-range magnetic order, either from the spin chirality of a paramagnetic state[7] or from fractionalized (topological) excitations in a spin liquid[11]. On the experimental side, a sizeable κ_{xy} has been measured in insulators without magnetic order, such as the spin-ice system $Tb_2Ti_2O_7$ (ref. [12]) and the spin-liquid systems $RuCl_3$ (ref. [4]), volborthite[5] and Ca kapellasite[6].

In cuprates, studies of κ_{xy} have so far been limited to the superconducting state[13–15], except for the case of $YBa_2Cu_3O_y$ (YBCO) at $p = 0.11$, where κ_{xy} was measured in the field-induced normal state[16], which has charge-density-wave order[2]. See Methods for a discussion of this particular case.

Here, we investigate the thermal Hall response of the pseudogap phase via measurements of κ_{xy} in four different cuprate

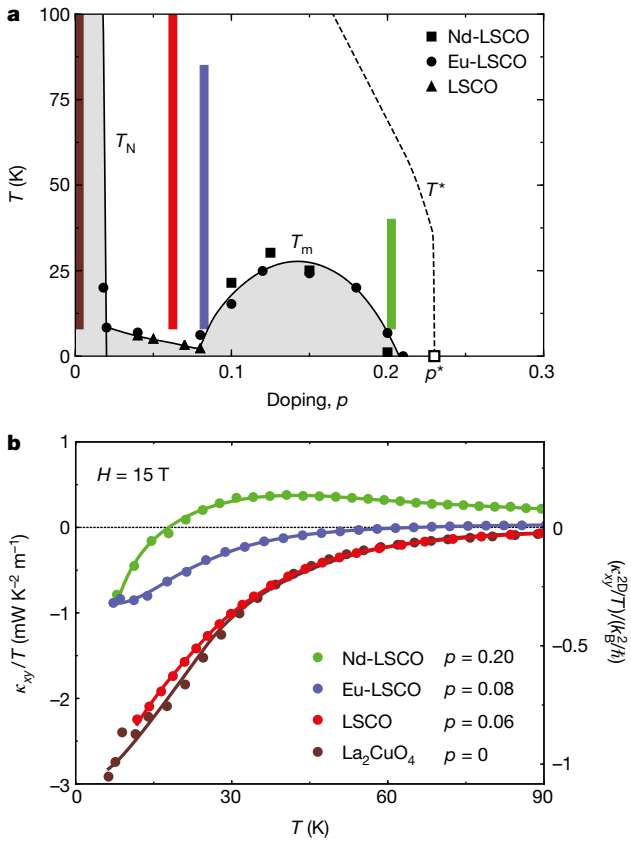

Fig. 1 | Phase diagram and thermal Hall conductivity of cuprates. **a**, Temperature–doping phase diagram of Nd-LSCO, Eu-LSCO and LSCO, showing the antiferromagnetic phase below the Néel temperature T_N and the pseudogap phase below T^* (ref. [29]), which ends at the critical doping $p^* = 0.23$ for both Nd-LSCO (ref. [17]) and Eu-LSCO (ref. [30]). For LSCO, $p^* \approx 0.18$ (ref. [29]). Short-range incommensurate spin order occurs below T_m, as measured by μSR on Nd-LSCO (squares[21]), Eu-LSCO (circles[31]) and LSCO (triangles[32]). The coloured vertical strips indicate the temperature range where the thermal Hall conductivity κ_{xy}/T at the corresponding doping decreases towards negative values at low temperature (see **b**). **b**, Thermal Hall conductivity κ_{xy}/T versus temperature in a field $H = 15$ T, for four materials and dopings as indicated, colour-coded with the vertical strips in **a**. On the right vertical axis, the magnitude of κ_{xy}/T is expressed in fundamental units of thermal conductance per plane ($k_B^2/\hbar$).

[1]Département de physique, Institut quantique, and RQMP, Université de Sherbrooke, Sherbrooke, Québec, Canada. [2]SPEC, CEA, CNRS-UMR3680, Université Paris-Saclay, Gif-sur-Yvette, France. [3]Materials Science and Engineering Program, Department of Mechanical Engineering, University of Texas at Austin, Austin, TX, USA. [4]Department of Advanced Materials Science, University of Tokyo, Kashiwa, Japan. [5]Department of Applied Physics, University of Tokyo, Tokyo, Japan. [6]Max Planck Institute for Solid State Research, Stuttgart, Germany. [7]Department of Physics, University of Tokyo, Tokyo, Japan. [8]Institute for Functional Matter and Quantum Technologies, University of Stuttgart, Stuttgart, Germany. [9]Central Research Institute of Electric Power Industry, Kanagawa, Japan. [10]Canadian Institute for Advanced Research, Toronto, Ontario, Canada. *e-mail: gael.grissonnanche@usherbrooke.ca; louis.taillefer@usherbrooke.ca

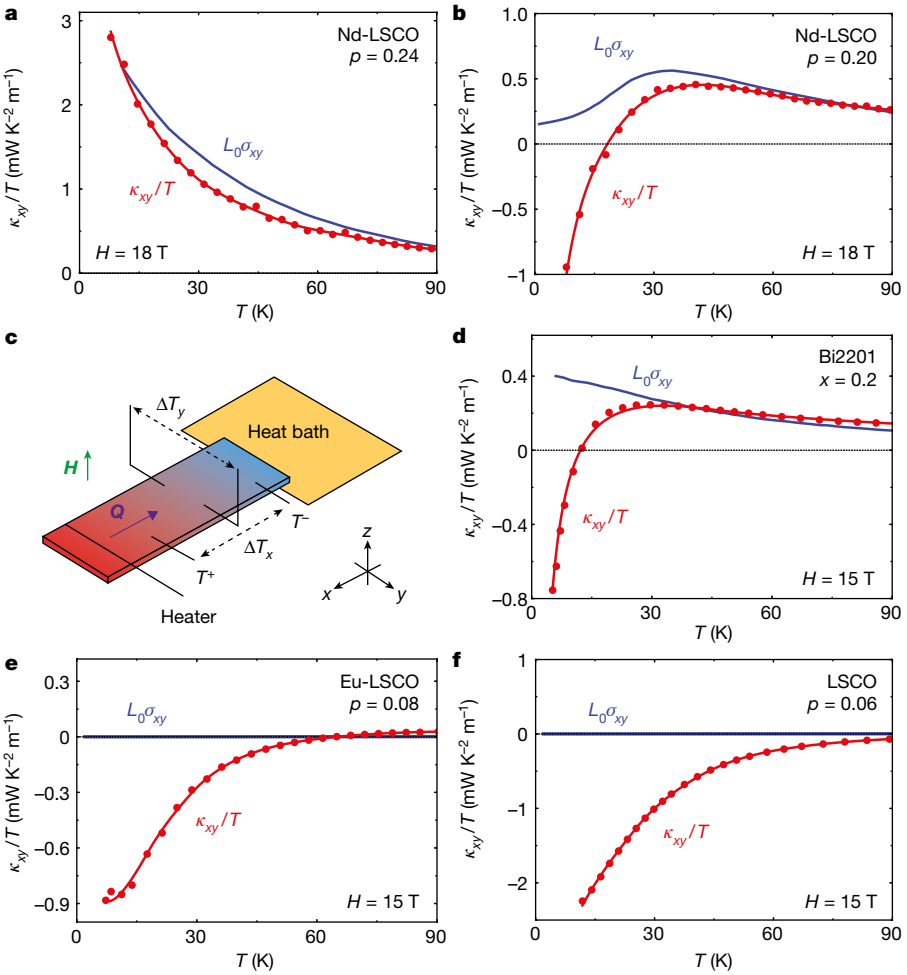

Fig. 2 | Thermal and electrical Hall conductivities of four cuprates. Data panels show thermal Hall conductivity κ_{xy}, plotted as κ_{xy}/T (red), and electrical Hall conductivity σ_{xy}, expressed as $L_0\sigma_{xy}$ (blue), where $L_0 = (\pi^2/3)(k_B/e)^2$, as a function of temperature: the material, its doping p and field H are indicated. **a**, **b**, Nd-LSCO; **c**, sketch of the thermal Hall measurement set-up (see Methods); **d**, Bi2201; **e**, Eu-LSCO; and **f**, LSCO. (For Nd-LSCO $p = 0.20$ (**b**), σ_{xy} was measured[17] at $H = 33$ T.) In Nd-LSCO at $p = 0.24$, κ_{xy}/T and $L_0\sigma_{xy}$ are both positive at all temperatures and they track each other, satisfying the Wiedemann–Franz law in the $T = 0$ limit. By contrast, for $p < p^*$ in all four materials, κ_{xy}/T falls to large and negative values at low temperature, whereas $L_0\sigma_{xy}$ remains positive.

materials—$La_{1.6-x}Nd_{0.4}Sr_xCuO_4$ (Nd-LSCO), $La_{1.8-x}Eu_{0.2}Sr_xCuO_4$ (Eu-LSCO), $La_{2-x}Sr_xCuO_4$ (LSCO) and $Bi_2Sr_{2-x}La_xCuO_{6+\delta}$ (Bi2201)—across a wide doping range, from the overdoped metal at $p = 0.24$ down to the Mott insulator at $p \approx 0$ (Fig. 1a). The κ_{xy} data reported here are all in the normal state, with superconductivity suppressed by application of a magnetic field normal to the CuO_2 planes.

In Nd-LSCO and Eu-LSCO, the critical doping[17] is at $p^* = 0.23$ (Fig. 1a). In Fig. 2a, we plot κ_{xy}/T versus T for Nd-LSCO at $p = 0.24$. We find that κ_{xy} is positive and that κ_{xy}/T increases monotonically with decreasing T, tracking closely the electrical Hall conductivity σ_{xy} measured on the same sample, satisfying the Wiedemann–Franz law as $T \to 0$, namely $\kappa_{xy}/T = L_0\sigma_{xy}$, where $L_0 = (\pi^2/3)(k_B/e)^2$ (here k_B is the Boltzmann constant and e the electron charge). The large positive value of σ_{xy} is dictated by the large Fermi surface at $p > p^*$ and its positive Hall number $n_H \approx 1 + p$ (ref. [17]). Clearly, at $p = 0.24$, κ_{xy} is entirely due to the conventional Hall effect of mobile charge carriers.

We now turn to dopings immediately below the pseudogap critical point. In Fig. 2b, we plot κ_{xy}/T versus T for Nd-LSCO at $p = 0.20$. We see a qualitatively different behaviour, with κ_{xy} becoming negative at low T. As seen in Fig. 3a, this qualitative change occurs immediately below p^*. In Eu-LSCO, the very same change occurs across p^* (Fig. 3b), from positive κ_{xy} above p^* ($p = 0.24$) to negative κ_{xy} (at low T) below p^* ($p = 0.21$), with essentially identical data to Nd-LSCO at $p = 0.24$ and $p = 0.21$. The negative κ_{xy} is therefore a property of the pseudogap phase.

We also measured κ_{xy} in Bi2201 (a cuprate with a different crystal structure to that of Nd-LSCO and Eu-LSCO), using an overdoped sample of La content $x = 0.2$, with p slightly below p^* (ref. [18]). In Fig. 2d, we see that $\kappa_{xy}(T)$ in Bi2201 displays a remarkably similar behaviour to that of Nd-LSCO and Eu-LSCO at $p < p^*$. A negative thermal Hall conductivity κ_{xy} at low temperature is therefore a generic property of the pseudogap phase, independent of material. Note that the electrical Hall conductivity σ_{xy} measured on the same samples remains positive down to $T \to 0$ (Fig. 2b, d).

We now move to much lower doping. In Fig. 1b, we see that κ_{xy}/T is still negative at low temperature in Eu-LSCO at $p = 0.08$ and in LSCO at $p = 0.06$, where in both cases σ_{xy} is positive and completely negligible (Fig. 2e, f), because the samples are almost electrically insulating at low temperature. This shows that the negative κ_{xy} signal of the pseudogap phase is not due to the conventional Hall effect of mobile charge carriers.

Magnons can be excluded as the source of this negative κ_{xy}. In the phase diagram of Fig. 1a, we delineate in grey the regions where static magnetism is detected by muon spin resonance (μSR), whether as incommensurate correlations below an onset temperature T_m or as commensurate Néel order below the Néel temperature, T_N. We see that in all three materials—Nd-LSCO at $p = 0.20$, Eu-LSCO at $p = 0.08$ and LSCO at $p = 0.06$—the negative κ_{xy} signal is present well above T_m (Fig. 1), where there is no static magnetism. Moreover, the $\kappa_{xy}(T)$ curve for La_2CuO_4 (Fig. 1b), that is, undoped LSCO with $p \approx 0$, where

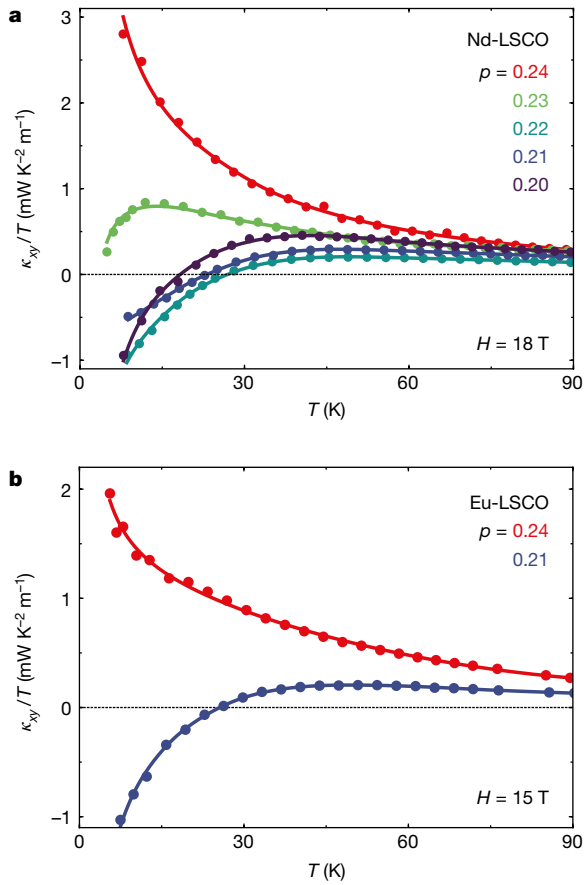

Fig. 3 | Thermal Hall conductivity across the pseudogap critical point *p.** Shown is thermal Hall conductivity κ_{xy}/T for Nd-LSCO in $H = 18$ T (**a**) and Eu-LSCO in $H = 15$ T (**b**), at dopings as indicated, on both sides of the pseudogap critical point $p^* = 0.23$. In both materials, κ_{xy} becomes negative at low temperature when $p < p^*$.

there is long-range antiferromagnetic order below approximately 300 K (Fig. 1a), is very similar to the curve for LSCO at $p = 0.06$ (Fig. 1b), where there is no magnetic order above $T \approx 5$ K (Fig. 1a). (See Methods for further discussion of magnons.) We conclude that magnetic order is not responsible for the negative κ_{xy} signal seen in cuprates at all dopings below p^*, and magnons are ruled out as the relevant excitations.

Phonons can generate a non-zero κ_{xy} signal if they are subject to scattering by spins[19,20]. Spin scattering will also show up in the longitudinal thermal conductivity κ_{xx}, which is dominated by phonons, in two ways: (1) it reduces the magnitude of κ_{xx} relative to a non-magnetic analogue material; and (2) it produces a field dependence of κ_{xx}.

In relation to (1), we note that κ_{xx} in Nd-LSCO does not decrease below p^*; on the contrary, it increases (Extended Data Fig. 3), most probably because electron–phonon scattering decreases as the charge carrier density drops. So the large negative κ_{xy} signal that appears below p^* is not accompanied by a reduction of κ_{xx} that would signal the onset of spin scattering. One could invoke a scenario where the decrease in electron–phonon scattering overcompensates the effect of the spin scattering, but the latter would still have to be small, which is hard to reconcile with the enormous κ_{xy} signal. Moreover, there is no evidence that the spin state of Nd-LSCO changes across p^*. On the contrary, static moments present at $p = 0.12$ cease to be detected (by μSR) at $p = 0.20$ (ref. [21]), so that $p = 0.20$ and $p = 0.24$ are equally non-magnetic from the μSR point of view. In other words, magnetic moments that could scatter phonons are not substantially different above and below p^*.

In relation to (2), the strength of the field (H) dependence of κ_{xx} is measured by the ratio $[\kappa_{xx}(H) - \kappa_{xx}(0)]/\kappa_{xx}(0)$. In Fig. 4a, we compare cuprates to various insulators with sizeable κ_{xy} signals. We see that the field dependence of κ_{xx} in LSCO $p = 0.06$, Eu-LSCO $p = 0.08$ and La_2CuO_4 is much smaller than in other materials, including $Ba_3CuSb_2O_9$ (ref. [20]) for example, a material where spin–phonon scattering generates the κ_{xy} signal. Although this could in part be due to a larger relevant field scale in cuprates, we are nonetheless left with little evidence of strong spin–phonon scattering in cuprates.

Given that the usual two indicators of a phonon-driven κ_{xy} are not clearly observed in our data, we conclude that phonons are unlikely to be responsible for the large negative κ_{xy} signal of cuprates that appears suddenly below p^*. (See Methods for further discussion.)

The κ_{xy} signal in the Mott insulator La_2CuO_4 is the largest seen so far in any insulator. Only multiferroic materials such as ferrimagnetic $(Fe,Zn)_2Mo_3O_8$ have comparable κ_{xy} values[3] (Fig. 4b), thanks to their exceptionally strong lattice–spin coupling—a measure of which is the strong field dependence of κ_{xx}, about 100 times larger in $(Fe,Zn)_2Mo_3O_8$ than in the cuprates (Fig. 4a).

The large negative κ_{xy} reported here for cuprates is not due to the standard Hall effect of charge carriers, it is not caused by magnons and there is no clear evidence that it comes from phonons. Its occurrence is all the more surprising given the 'no-go theorem' that should strongly limit its magnitude on a square lattice[22]. Identifying the excitations responsible for the negative κ_{xy} signal will shed new light on the nature of the pseudogap phase. It is instructive to compare cuprates with insulators that are believed to host spin-liquid states. The largest κ_{xy} signal so far in such materials was detected in $RuCl_3$ (Fig. 4b). In this 2D

Table 1 | Thermal Hall conductivity in various insulators

Material	κ_{xy} (mW K^{-1} m^{-1})	κ_{xx} (W K^{-1} m^{-1})	$\lvert\Delta\kappa_{xx}\rvert$ (W K^{-1} m^{-1})	$\lvert\Delta\kappa_{xx}/\kappa_{xx}\rvert$	T (K)	H (T)	Reference
La_2CuO_4	−38.6	12.4	~0.06	~0.005	20	15	This work
LSCO	−30.0	5.1	~0.02	~0.004	15	15	This work
Eu-LSCO	−13.2	4.5	~0.015	~0.003	15	15	This work
$Lu_2V_2O_7$	1.0	0.75	ND	ND	50	9	[28]
$Fe_2Mo_3O_8$	24	9	5	0.55	45	14	[3]
$(Fe,Zn)_2Mo_3O_8$	24	10	3.2	0.32	30	9	[3]
$Tb_2Ti_2O_7$	1.2	0.37	0.12	0.32	15.5	8	[12]
$RuCl_3$	8	15.5	0.62	0.04	20	15	[4]
$RuCl_3$	3.5	8	0.45	0.055	35	16	[23]
Ca kapellasite	1.1	0.2	ND	ND	16	15	[6]
$Ba_3CuSb_2O_9$	0.008	0.07	0.0035	0.05	5	15	[20]

Maximal value of the thermal Hall conductivity κ_{xy} (second column) in various insulators (first column), compared to our three cuprates (the first three entries, namely, La_2CuO_4, LSCO $p = 0.06$ and Eu-LSCO $p = 0.08$), measured at temperature T and field H as indicated (columns 6 and 7 respectively): the ferromagnet $Lu_2V_2O_7$ (ref. [28]); the multiferroic ferrimagnets $Fe_2Mo_3O_8$ and $(Fe_{0.875}Zn_{0.125})_2Mo_3O_8$ (ref. [3]); the spin-ice material $Tb_2Ti_2O_7$ (ref. [12]); and the spin-liquid candidates $RuCl_3$ (refs [4,23]), Ca kapellasite[6] and $Ba_3CuSb_2O_9$ (ref. [20]). We also list the thermal conductivity κ_{xx} measured at the same temperature, in zero field (third column). The change induced in κ_{xx} by the field, $\Delta\kappa_{xx} = \kappa_{xx}(H) - \kappa_{xx}(0)$, is given in absolute and relative terms (fourth and fifth column, respectively). ND, not determined.

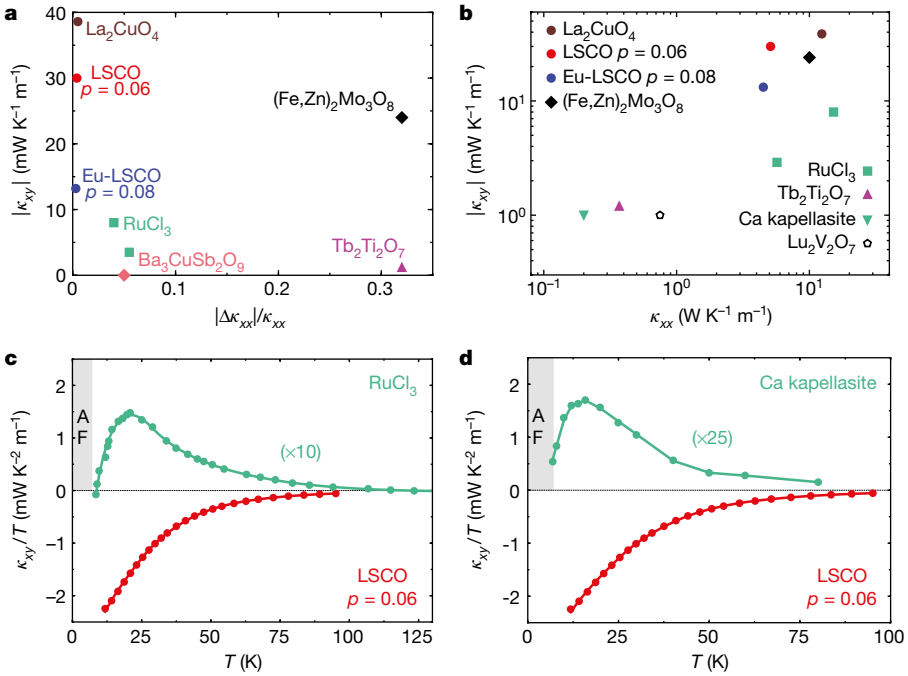

Fig. 4 | Comparison with other insulators, including spin-liquid candidates. a, **b**, Maximal absolute value of κ_{xy} in various insulators, including the multiferroic ferrimagnet $(Fe,Zn)_2Mo_3O_8$ (black diamond[3]; the previous record holder for the largest $|\kappa_{xy}|$ of any insulator) and the spin-liquid insulator $RuCl_3$ (green squares[4,23]; the previous record holder for the largest $|\kappa_{xy}|$ of any insulator without magnetic order). **a**, Maximal $|\kappa_{xy}|$ as a function of the corresponding value of $[\kappa_{xx}(H) - \kappa_{xx}(0)]/\kappa_{xx}(0)$. **b**, Maximal $|\kappa_{xy}|$ as a function of the corresponding κ_{xx} value, on a log–log plot. The values for all materials are listed in Table 1. We see that La_2CuO_4 has the largest known value of all insulators. **c**, Thermal Hall conductivity κ_{xy}/T versus temperature for LSCO at $p = 0.06$ in $H = 15$ T (red) and $RuCl_3$ in $H = 16$ T (blue, ×10; data from ref. [23]). In $RuCl_3$, the gradual growth of κ_{xy}/T on cooling below $T \approx 100$ K is attributed to Majorana fermions, the topological excitations of the Kitaev spin liquid[4,6,11]. Below $T \approx 20$ K, κ_{xy}/T drops on approaching the antiferromagnetic phase (AF; grey). **d**, Same as in **c** but for the spin-liquid insulator Ca kapellasite (green, ×25; data from ref. [6]). These comparisons point to a spin-liquid character of the pseudogap phase in cuprates.

material, spins on a honeycomb lattice are frustrated and only order (antiferromagnetically) below $T_N = 7$ K. Above T_N, the paramagnetic state is thought to be a spin-liquid state described approximately by the Kitaev model[11]. In Fig. 4c, we reproduce data from ref. [23] for κ_{xy}/T versus T in $RuCl_3$. Above 100 K, κ_{xy}/T is vanishingly small. Below 100 K, κ_{xy}/T grows gradually with decreasing T down to 20 K or so (and then drops rapidly as T_N is approached). In the regime between 20 K and 100 K, κ_{xy}/T is well described by calculations for the Kitaev model[11], implying that the κ_{xy} signal in $RuCl_3$ comes from itinerant Majorana fermions—exotic neutral excitations of topological character. This interpretation is supported by the observation[24] of a predicted[11] quantization of the thermal Hall conductivity (at low T when antiferromagnatic order is suppressed by applying a field in the 2D planes). Other spin-liquid candidates, such as volborthite[5] and Ca kapellasite[6], exhibit qualitatively similar $\kappa_{xy}(T)$ (Fig. 4d), suggesting that the gradual growth below about 100 K is a general behaviour.

In Fig. 4c, d, we compare our data on LSCO $p = 0.06$ to the data on $RuCl_3$ and Ca kapellasite, respectively. There is a tantalizing similarity in the gradual growth of $|\kappa_{xy}/T|$ below 100 K or so, but there are some differences. First, whereas κ_{xy} is positive in these two spin-liquid candidates, it is negative in cuprates. (This may reflect the particular topological character of the different states.) Second, the signal in LSCO is approximately 10 to 25 times larger (Fig. 4). Last, in LSCO, κ_{xy}/T continues to grow down to the lowest measured temperature (but it may well drop below about 5–10 K).

In summary, the thermal Hall effect in cuprates reveals a hitherto unknown facet of both the enigmatic pseudogap phase and the Mott insulator, reminiscent of a spin liquid. It points to a state with chirality[7]. It will be interesting to see whether models of topological order[10], spin–charge separation[25] or current loops[26], for example, may be consistent with the giant κ_{xy} signal that appears below p^*. A recent calculation shows that neutral spinons in certain states with topological order on a square lattice can produce a substantially enhanced thermal Hall conductivity[27].

Online content

Any methods, additional references, Nature Research reporting summaries, source data, statements of data availability and associated accession codes are available at https://doi.org/10.1038/s41586-019-1375-0.

Received: 18 December 2018; Accepted: 26 April 2019;
Published online 17 July 2019.

1. Keimer, B. et al. From quantum matter to high-temperature superconductivity in copper oxides. *Nature* **518**, 179–186 (2015).
2. Proust, C. & Taillefer, L. The remarkable underlying ground states of cuprate superconductors. *Annu. Rev. Condens. Matter Phys.* **10**, 409–429 (2019).
3. Ideue, T. et al. Giant thermal Hall effect in multiferroics. *Nat. Mater.* **16**, 797–802 (2017).
4. Kasahara, Y. et al. Unusual thermal Hall effect in a Kitaev spin liquid candidate α-$RuCl_3$. *Phys. Rev. Lett.* **120**, 217205 (2018).
5. Watanabe, D. et al. Emergence of nontrivial magnetic excitations in a spin-liquid state of kagomé volborthite. *Proc. Natl Acad. Sci. USA* **113**, 8653–8657 (2016).
6. Doki, H. et al. Spin thermal Hall conductivity of a Kagome antiferromagnet. *Phys. Rev. Lett.* **121**, 097203 (2018).
7. Lee, H., Han, J. H. & Lee, P. A. Thermal Hall effect of spins in a paramagnet. *Phys. Rev. B* **91**, 125413 (2015).
8. Monthoux, P., Pines, D. & Lonzarich, G. G. Superconductivity without phonons. *Nature* **450**, 1177–1183 (2007).
9. Kyung, B. et al. Pseudogap induced by short-range spin correlations in a doped Mott insulator. *Phys. Rev. B* **73**, 165114 (2006).
10. Scheurer, M. S. et al. Topological order in the pseudogap metal. *Proc. Natl Acad. Sci. USA* **115**, E3665–E3672 (2018).
11. Nasu, J., Yoshitake, J. & Motome, Y. Thermal transport in the Kitaev model. *Phys. Rev. Lett.* **119**, 127204 (2017).
12. Hirschberger, M. et al. Large thermal Hall conductivity of neutral spin excitations in a frustrated quantum magnet. *Science* **348**, 106–109 (2015).
13. Zhang, Y. et al. Giant enhancement of the thermal Hall conductivity κ_{xy} in the superconductor $YBa_2Cu_3O_7$. *Phys. Rev. Lett.* **86**, 890–893 (2001).
14. Durst, A. C., Vishwanath, A. & Lee, P. A. Weak-field thermal Hall conductivity in the mixed state of d-wave superconductors. *Phys. Rev. Lett.* **90**, 187002 (2003).
15. Cvetkovic, V. & Vafek, O. Berry phases and the intrinsic thermal Hall effect in high-temperature cuprate superconductors. *Nat. Commun.* **6**, 6518 (2015).
16. Grissonnanche, G. et al. Wiedemann-Franz law in the underdoped cuprate superconductor $YBa_2Cu_3O_y$. *Phys. Rev. B* **93**, 064513 (2016).

17. Collignon, C. et al. Fermi-surface transformation across the pseudogap critical point of the cuprate superconductor $La_{1.6-x}Nd_{0.4}Sr_xCuO_4$. *Phys. Rev. B* **95**, 224517 (2017).
18. Kawasaki, S. et al. Carrier-concentration dependence of the pseudogap ground state of superconducting $Bi_2Sr_{2-x}La_xCuO_6$ revealed by ^{63,65}Cu-nuclear magnetic resonance in very high magnetic fields. *Phys. Rev. Lett.* **105**, 137002 (2010).
19. Strohm, C., Rikken, G. L. J. A. & Wyder, P. Phenomenological evidence for the phonon Hall effect. *Phys. Rev. Lett.* **95**, 155901 (2005).
20. Sugii, K. et al. Thermal Hall effect in a spin-phonon glass $Ba_3CuSb_2O_9$. *Phys. Rev. Lett.* **118**, 145902 (2017).
21. Nachumi, B. et al. Muon spin relaxation study of the stripe phase order in $La_{1.6-x}Nd_{0.4}Sr_xCuO_4$ and related 214 cuprates. *Phys. Rev. B* **58**, 8760–8772 (1998).
22. Katsura, H., Nagaosa, N. & Lee, P. A. Theory of the thermal Hall effect in quantum magnets. *Phys. Rev. Lett.* **104**, 066403 (2010).
23. Hentrich, R. et al. Large thermal Hall effect in α-$RuCl_3$: evidence for heat transport by Kitaev-Heisenberg paramagnons. *Phys. Rev. B* **99**, 085136 (2019).
24. Kasahara, Y. et al. Majorana quantization and half-integer thermal quantum Hall effect in a Kitaev spin liquid. *Nature* **559**, 227–231 (2018).
25. Kivelson, S. A., Rokhsar, D. S. & Sethna, J. P. Topology of the resonating valence-bond state: solitons and high-T_c superconductivity. *Phys. Rev. B* **35**, 8865 (1987).
26. Varma, C. M. Theory of the pseudogap state of the cuprates. *Phys. Rev. B* **73**, 155113 (2006).
27. Samajdar, R., Chatterjee, S., Sachdev, S. & Scheurer, M. Thermal Hall effect in square-lattice spin liquids: a Schwinger boson mean-field study. *Phys. Rev. B* **99**, 165126 (2019).
28. Onose, Y. et al. Observation of the magnon Hall effect. *Science* **329**, 297–299 (2010).
29. Cyr-Choinière, O. et al. Pseudogap temperature T^* of cuprate superconductors from the Nernst effect. *Phys. Rev. B* **97**, 064502 (2018).
30. Michon, B. et al. Thermodynamic signatures of quantum criticality in cuprate superconductors. *Nature* **567**, 218–222 (2019).
31. Klauss, H.-H. et al. From antiferromagnetic order to static magnetic stripes: the phase diagram of $(La, Eu)_{2-x}Sr_xCuO_4$. *Phys. Rev. Lett.* **85**, 4590–4593 (2000).
32. Hücker, M. et al. Coupling of stripes to lattice distortions in cuprates and nickelates. *Physica C* **460–462**, 170–173 (2007).

Acknowledgements We thank L. Balents, K. Behnia, S. Chatterjee, B. D. Gaulin, H. J. Han, S. M. Hayden, C. Hess, S. A. Kivelson, H. Y. Kee, P. A. Lee, Y. S. Lee, A. Rosch, S. Sachdev, M. Scheurer, T. Senthil, A.-M. S. Tremblay, C. M. Varma and S. Verret for helpful and stimulating discussions. L.T. acknowledges support from the Canadian Institute for Advanced Research (CIFAR) as a CIFAR Fellow and funding from the Natural Sciences and Engineering Research Council of Canada (NSERC), the Fonds de recherche du Québec–Nature et Technologies (FRQNT), the Canada Foundation for Innovation (CFI), and a Canada Research Chair. This research was undertaken thanks in part to funding from the Canada First Research Excellence Fund. Part of this work was funded by the Gordon and Betty Moore Foundation's EPiQS Initiative (grant GBMF5306 to L.T.). J.-S.Z was supported by NSF MRSEC DMR-1720595 in the US.

Reviewer information *Nature* thanks Kwang-yong Choi, Patrick Lee and the other anonymous reviewer(s) for their contribution to the peer review of this work.

Author contributions G.G., A.L., S.B., E.L., V.Z., M.L., F.L., A.G. and N.D.-L. performed the thermal Hall conductivity measurements. G.G., A.L., S.B., E.L., V.Z., M.L. and N.D.-L. performed the electrical Hall conductivity measurements. J.-S.Z. grew the Nd-LSCO single crystals. S.P., T.T. and H.T. grew the Eu-LSCO and LSCO single crystals. S.O. grew the Bi2201 single crystal. G.G., N.D.-L. and L.T. wrote the manuscript, in consultation with all authors. L.T. supervised the project.

Competing interests The authors declare no competing interests.

Additional information
Extended data figures and tables is available for this paper at https://doi.org/10.1038/s41586-019-1375-0.
Reprints and permissions information is available at http://www.nature.com/reprints.
Correspondence and requests for materials should be addressed to G.G. or L.T.
Publisher's note: Springer Nature remains neutral with regard to jurisdictional claims in published maps and institutional affiliations.

METHODS

Samples. *Nd-LSCO.* Single crystals of $La_{2-y-x}Nd_ySr_xCuO_4$ (Nd-LSCO) were grown at the University of Texas at Austin using a travelling-float-zone technique, with a Nd content $y = 0.4$ and nominal Sr concentrations $x = 0.20$, 0.21, 0.22, 0.23 and 0.25. The hole concentration p is given by $p = x$, with an error bar ± 0.003, except for the $x = 0.25$ sample, for which the doping is $p = 0.24 \pm 0.005$ (for more details, see ref. [17]). The value of T_c, defined as the point of zero resistance, is $T_c = 15.5$, 15, 14.5, 12 and 11 K for samples with $x = 0.20$, 0.21, 0.22, 0.23 and 0.24, respectively. The pseudogap critical point in Nd-LSCO is at $p^* = 0.23$ (ref. [17]).

Eu-LSCO. Single crystals of $La_{2-y-x}Eu_ySr_xCuO_4$ (Eu-LSCO) were grown at the University of Tokyo using a travelling-float-zone technique, with a Eu content $y = 0.2$ and nominal Sr concentrations $x = 0.08$, 0.21 and 0.24. The hole concentration p is given by $p = x$, with an error bar of ± 0.005. The value of T_c, defined as the point of zero resistance, is $T_c = 3$, 14 and 9 K for samples with $x = 0.08$, 0.21 and 0.24, respectively. The pseudogap critical point in Eu-LSCO is at $p^* = 0.23$ (ref. [30]).

LSCO. Single crystals of $La_{2-x}Sr_xCuO_4$ (LSCO) were grown at the University of Tokyo using a travelling-float-zone technique, with nominal Sr concentrations $x = 0.0$ (that is, La_2CuO_4) and 0.06. The hole concentration p is $p \approx 0$ and $p = 0.06 \pm 0.005$, respectively. The value of T_c, defined as the point of zero resistance, is $T_c = 0$ and 5 K for samples with $x = 0.0$ and 0.06, respectively. The pseudogap critical point in LSCO is at $p^* \approx 0.18$ (ref. [29]).

Bi2201. Our single crystal of $Bi_2Sr_{2-x}La_xCuO_{6+\delta}$ (Bi2201) was grown at CRIEPI in Kanagawa using a travelling-float-zone technique[33], with La content $x = 0.2$. The value of T_c, defined as the onset of the drop in magnetization, is $T_c = 18$ K. Given its x and T_c values, the doping of this overdoped sample is such that $p < p^*$ (ref. [18]).

Transport measurements. Our comparative study of heat and charge transport was performed by measuring the thermal Hall conductivity κ_{xy} and the electrical Hall conductivity σ_{xy} on the same sample, using the same contacts made of silver epoxy H20E annealed at high temperature in oxygen.

Thermal measurements. A constant heat current $\boldsymbol{Q}$ was sent in the basal plane of the single crystal (along x), generating a longitudinal temperature difference $\Delta T_x = T^+ - T^-$ (Fig. 2c). The thermal conductivity along the x axis is given by $\kappa_{xx} = (Q/\Delta T_x)(L/wt)$, where L is the separation (along x) between the two points at which T^+ and T^- are measured, w is the width of the sample (along y) and t its thickness (along z). By applying a magnetic field $\boldsymbol{H}$ along the c axis of the crystal (along z), normal to the CuO_2 planes, one generates a transverse gradient ΔT_y (Fig. 2c). The thermal Hall conductivity is defined as $\kappa_{xy} = -\kappa_{yy}(\Delta T_y/\Delta T_x)(L/w)$, where κ_{yy} is the longitudinal thermal conductivity along the y axis. In this study, we take $\kappa_{yy} = \kappa_{xx}$. The thermal Hall conductivity κ_{xy} of our samples was measured in magnetic fields up to $H = 18$ T. The measurement procedure is described in detail elsewhere[16].

Electrical measurements. The longitudinal resistivity ρ_{xx} and Hall resistivity ρ_{xy} were measured in magnetic fields up to 16 T in a Quantum Design PPMS in Sherbrooke. (For Nd-LSCO $p = 0.20$, σ_{xy} was measured at $H = 33$ T (ref. [17]).) The measurements were performed using a conventional six-point configuration with a current excitation of 2 mA, using the same contacts as for the thermal measurements (Fig. 2c). The electrical Hall conductivity σ_{xy} is given by $\sigma_{xy} = \rho_{xy}/(\rho_{xx}^2 + \rho_{xy}^2)$.

Field dependence of the thermal Hall conductivity. All of the data reported here were taken in a magnetic field (normal to the CuO_2 planes) large enough to fully suppress superconductivity, and thereby access the normal state of Nd-LSCO, Eu-LSCO, LSCO and Bi2201. Indeed, a field of 15 T is sufficient to do this in all samples presented here, down to at least 5 K. In the normal state, κ_{xy} has an intrinsic field dependence. In Extended Data Fig. 4, we show how κ_{xy} in LSCO $p = 0.06$, where $T_c = 5$ K, depends on magnetic field for $T > T_c$: the linear H dependence of κ_{xy} at high T becomes sublinear at low T.

It may be worth pointing out that the sudden appearance of a new negative κ_{xy} signal below p^* is not correlated with any change in the superconducting properties of the sample. The easiest way to see this is to compare Nd-LSCO or Eu-LSCO at $p = 0.24$ and $p = 0.21$. While the superconducting properties at $p = 0.24$ and $p = 0.21$ are very similar—that is, $T_c \approx 10$ K versus 15 K and $H_{c2} \approx 10$ T versus 15 T (ref. [30])—the κ_{xy} response is totally different (at low T): positive at $p = 0.24$, negative at $p = 0.21$ (Fig. 3).

Thermal Hall conductivity in YBCO. In YBCO at $p = 0.11$, there is huge negative κ_{xy} signal in the field-induced normal state[2]. In this excellent metal, whose Fermi surface is reconstructed by charge-density-wave order into a small electron pocket of high mobility[2], the electrical Hall conductivity σ_{xy} is equally huge. In fact, the Wiedemann–Franz law was found to hold, namely $\kappa_{xy}/T = L_0\sigma_{xy}$ as $T \to 0$, within error bars of $\pm 15\%$ (ref. [16]). In other words, the negative κ_{xy} signal in this case is due to the charge carriers (that is, to electrons). However, because the $\pm 15\%$ uncertainty corresponds to ± 12 mW K^{-2} m^{-1} (in 27 T), it is impossible to know whether the κ_{xy} signal in YBCO might also contain a contribution of -2 to -6 mW K^{-2} m^{-1} from neutral excitations (that is, -1 to -3 mW K^{-2} m^{-1} in 15 T; Fig. 1b).

Mott insulator. We can estimate the doping of our LCO sample (La_2CuO_4) by comparing its resistivity with published data. In Extended Data Fig. 6, we compare the resistivity of our LCO sample to published data by Uchida and co-workers[34] on the most stoichiometric sample of La_2CuO_4 they were able to produce, with the highest resistivity. We see that our LCO sample has a similar resistivity, even slightly higher at low temperature. We conclude that p is very close to zero in our sample. In Extended Data Fig. 6, we also compare with data from Komiya and co-workers[35] on a LSCO sample with Sr content $x = 0.01$. We see that our LCO sample's resistivity is larger by several orders of magnitude. We conclude that $p < 0.01$ in our LCO sample.

In Extended Data Fig. 6, we compare the resistivity of our sample of LCO and our sample of LSCO with $p = 0.06$. We see that their resistivities at low T differ by 7–8 orders of magnitude. This shows that although the two samples have very similar κ_{xy} curves (Fig. 1b), they are electrically very different.

Thermal Hall signal from magnons. In undoped La_2CuO_4, magnons have been well characterized by inelastic neutron scattering measurements[36]. There are two magnon branches, each with its own spin gap, of magnitude 26 K and 58 K, respectively. The thermal conductivity of magnons, κ_{mag}, is therefore thermally activated at $T < 26$ K, so that κ_{mag} decreases exponentially at low T. Hess and co-workers have estimated κ_{mag} in La_2CuO_4 by taking the difference between in-plane and out-of-plane conductivities[37]. In Extended Data Fig. 5, we see that κ_{mag}/T decreases monotonically as $T \to 0$ below 150 K.

By contrast, κ_{xy}/T in La_2CuO_4 increases monotonically with decreasing T, all the way down to $T \approx 5$ K (Extended Data Fig. 5), a temperature 5 times smaller than the smallest gap, where there are no thermally excited magnons. Moreover, when we move up in doping to $p = 0.06$, where antiferromagnetic order is gone and LSCO is in a very different magnetic state (Fig. 1a), without well-defined magnons or a spin gap, $\kappa_{xy}(T)$ is essentially identical to that in La_2CuO_4 (Fig. 1b). We conclude that magnons are not responsible for the large negative κ_{xy} in cuprates.

Note, moreover, that a collinear antiferromagnetic order on a square lattice (such as that found in La_2CuO_4) is expected[22] to yield $\kappa_{xy} = 0$. A non-zero κ_{xy} signal could come from the canting of spins out of the CuO_2 planes, but one would expect it to be very small[27]—and it would still vanish at low T because of the gap in the magnon spectrum. Note also that there could be some low-energy spin excitations in La_2CuO_4 besides the well-known magnons. Magnetic susceptibility measurements in La_2CuO_4 and lightly doped LSCO have revealed some unusual features, not consistent with a simple Néel state[38].

Thermal Hall signal from phonons. Phonons can produce a non-zero κ_{xy} signal if they undergo scattering by spins[3,19]. Spin scattering of phonons can be detected through its impact on κ_{xx}. First, it reduces the magnitude of κ_{xx} relative to its value without spin scattering. A good example of this is provided by the insulators $Y_2Ti_2O_7$ and $Tb_2Ti_2O_7$. In non-magnetic $Y_2Ti_2O_7$, $\kappa_{xx}(T)$ is large and typical of phonons in non-magnetic insulators (Extended Data Fig. 2a). In isostructural $Tb_2Ti_2O_7$, which has a large moment on the Tb ion, $\kappa_{xx}(T)$ is massively reduced (Extended Data Fig. 2a), as phonons undergo strong spin scattering. At $T = 15$ K, κ_{xx} is 15 times smaller in $Tb_2Ti_2O_7$.

A second signature of the spin scattering of phonons is a field dependence of κ_{xx}. In $Tb_2Ti_2O_7$, a field of 8 T causes a 30% reduction in κ_{xx} at $T = 15$ K (ref. [12]; Fig. 4a, Extended Data Fig. 2b, Table 1). In the multiferroic material $(Fe,Zn)_2Mo_3O_8$, where the spin–phonon coupling is known to be very strong, a field of 9 T causes a 30% reduction in κ_{xx} at $T = 30$ K (ref. [3]; Fig. 4a, Table 1).

Let us now look for those two signatures in cuprates. First, in Nd-LSCO, where the negative κ_{xy} signal is absent at $p = 0.24$ and present at $p = 0.21$, with a magnitude about 10 times larger than in $Tb_2Ti_2O_7$. If this very large κ_{xy} signal is due to phonons, then there must be some very strong spin scattering of phonons that appears below $p = 0.24$, which would show up as a massive decrease in κ_{xx}. In Extended Data Fig. 3, we see that there is no decrease of κ_{xx} in going from $p = 0.24$ to $p = 0.21$—on the contrary, κ_{xx} increases.

Second, we look at the field dependence of κ_{xx} in LSCO $p = 0.06$, where the negative κ_{xy} signal is about 20 times larger than in $Tb_2Ti_2O_7$, at $T = 15$ K and $H = 8$ T (ref. [12]; Extended Data Fig. 2b, d, Table 1). In LSCO, the change in κ_{xx} induced by a field of 8 T at $T = 14$ K is no more than 1% (Extended Data Figs. 1e and 2d), so about 20 times smaller than in $Tb_2Ti_2O_7$. (This could in part be due to a larger relevant field scale in cuprates.) In addition to being negligible in size, the H dependence of κ_{xx} in LSCO has the wrong T dependence: $[\kappa_{xx}(15\text{ T}) - \kappa_{xx}(1\text{ T})]/T$ drops below 30 K, whereas κ_{xy}/T keeps growing monotonically as $T \to 0$ (Extended Data Fig. 1f).

So we find that neither of the two standard signatures of strong phonon–spin scattering is clearly present in cuprates. Moreover, there is no evidence that a new spin state appears below p^* in Nd-LSCO, which would introduce a new mechanism for scattering phonons. On the contrary, static moments present at $p = 0.12$ cease to be detected (by μSR) at $p = 0.20$ (ref. [21]), so that $p = 0.20$ and $p = 0.24$ are equally non-magnetic from the μSR point of view.

We conclude that there is no clear evidence to suggest that phonons are responsible for the large negative κ_{xy} in cuprates that appears below p^*.

Data availability

The data that support the plots within this paper and other findings of this study are available from the corresponding authors upon reasonable request.

33. Ono, S. & Ando, Y. Evolution of the resistivity anisotropy in $Bi_2Sr_{2-x}La_xCuO_{6+\delta}$ single crystals for a wide range of hole doping. *Phys. Rev. B* **67**, 104512 (2003).
34. Uchida, S. et al. Electric and magnetic properties of La_2CuO_4. *Jpn. J. Appl. Phys.* **26**, L445 (1987).
35. Komiya, S., Ando, Y., Sun, X. F. & Lavrov, A. N. c-axis transport and resistivity anisotropy of lightly to moderately doped $La_{2-x}Sr_xCuO_4$ single crystals: implications on the charge transport mechanism. *Phys. Rev. B* **65**, 214535 (2002).
36. Keimer, B. et al. Soft phonon behavior and magnetism at the low temperature structural phase transition of $La_{1.65}Nd_{0.35}CuO_4$. *Z. Phys. B* **91**, 373–382 (1993).
37. Hess, C. et al. Magnon heat transport in doped La_2CuO_4. *Phys. Rev. Lett.* **90**, 197002 (2003).
38. Lavrov, A. N., Ando, Y., Komiya, S. & Tsukada, I. Unusual magnetic susceptibility anisotropy in untwinned $La_{2-x}Sr_xCuO_4$ single crystals in the lightly doped region. *Phys. Rev. Lett.* **87**, 017007 (2001).
39. Li, Q. J. et al. Phonon-glass-like behavior of magnetic origin in single crystal $Tb_2Ti_2O_7$. *Phys. Rev. B* **87**, 214408 (2013).
40. Michon, B. et al. Wiedemann-Franz law and abrupt change in conductivity across the pseudogap critical point of a cuprate superconductor. *Phys. Rev. X* **8**, 041010 (2018).

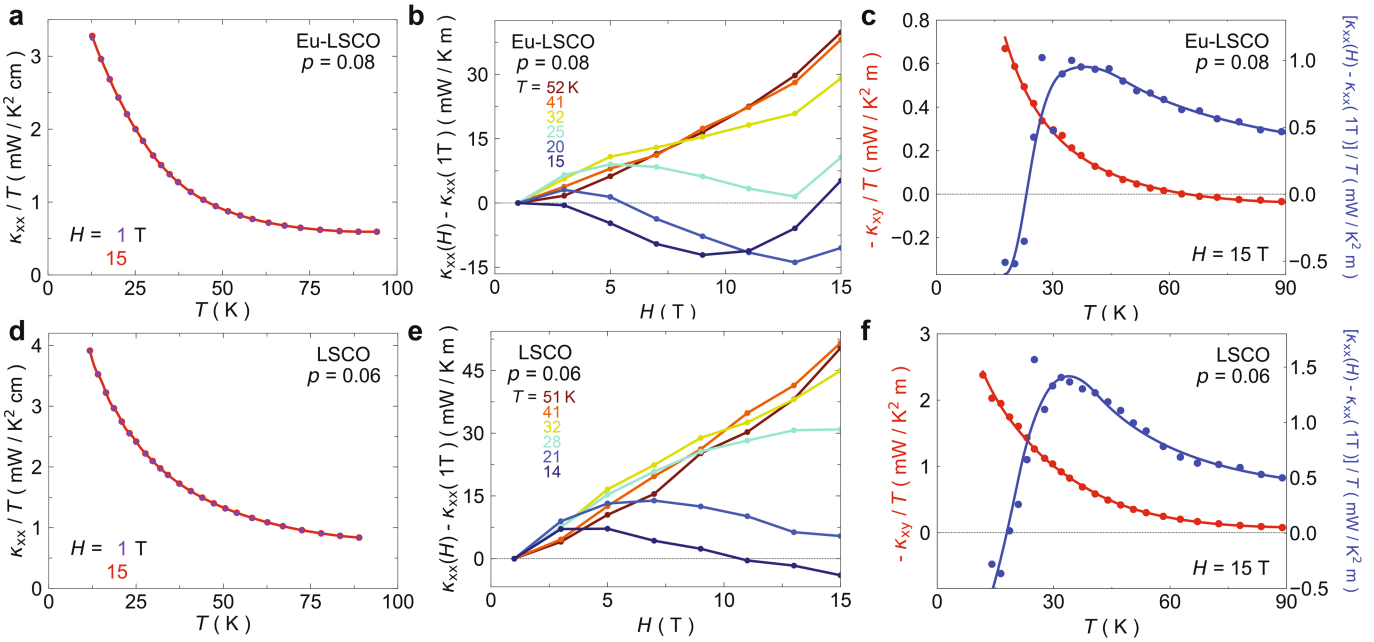

Extended Data Fig. 1 | Magnetic field dependence of κ_{xx}. a–f, Field dependence of κ_{xx} in Eu-LSCO $p = 0.08$ (top panels) and LSCO $p = 0.06$ (bottom panels), displayed in three ways. **a**, **d**, Plot of κ_{xx}/T versus T at $H = 1$ T (blue) and $H = 15$ T (red) (data points). The difference between the two curves is very small, not visible by eye. **b**, **e**, Plot of the change in κ_{xx} with field measured relative to its value at $H = 1$ T, that is, $[\kappa_{xx}(H) - \kappa_{xx}(1\text{ T})]$ versus H, for various temperatures as indicated (data points). **c**, **f**, Change in κ_{xx} between 15 T and 1 T, plotted as $[\kappa_{xx}(H) - \kappa_{xx}(1\text{ T})]/T$ versus T (blue, right axis), compared to $\kappa_{xy}(15\text{ T})/T$ versus T (red, left axis) (data points). Markers represent data and the line is a guide to the eye. Note how at low T the transverse response grows to be as large, if not larger, than the longitudinal response.

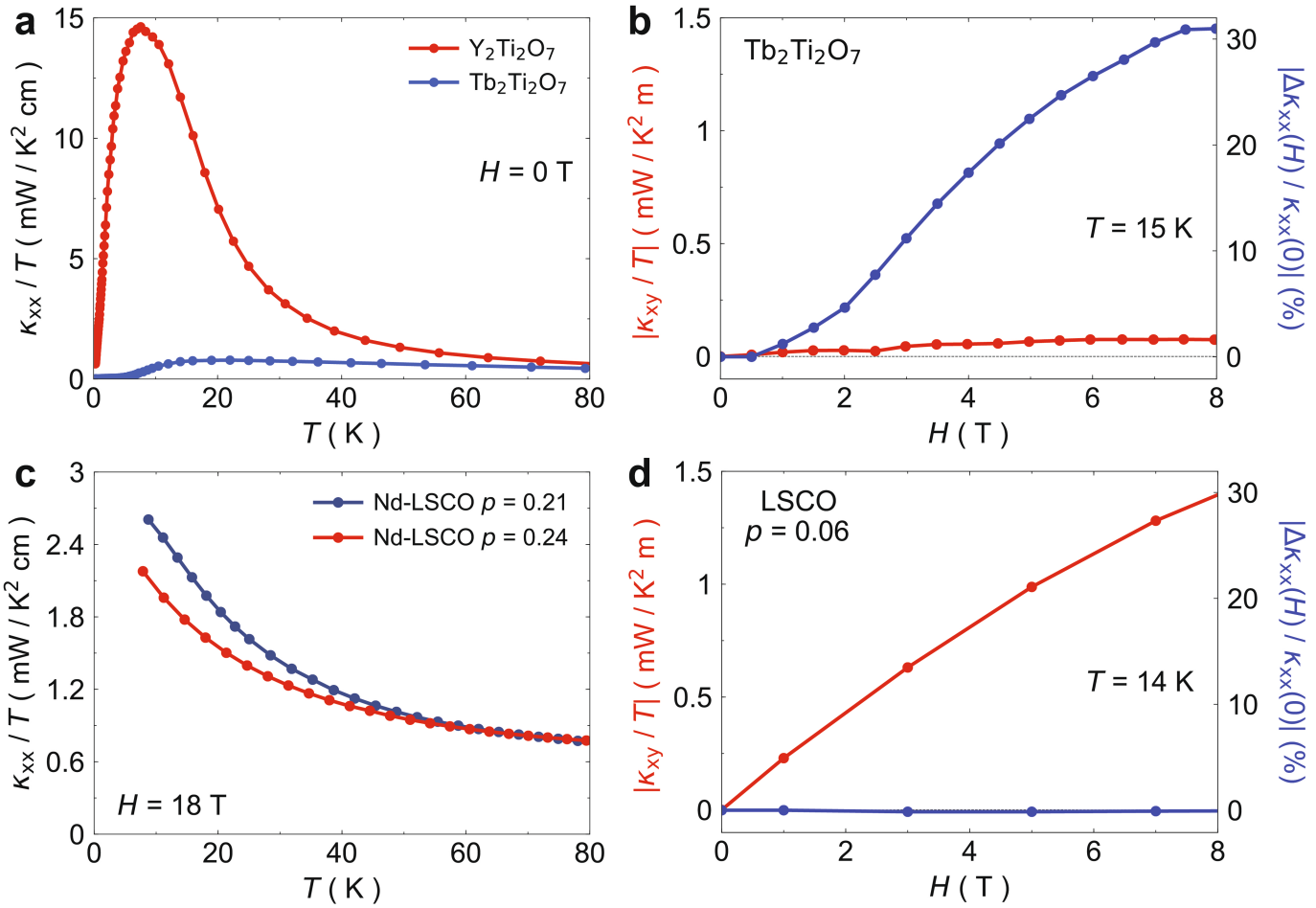

Extended Data Fig. 2 | Comparison of cuprates to other oxides. a, Thermal conductivity of two isostructural oxides, plotted as κ_{xx}/T versus T at $H = 0$, namely $Y_2Ti_2O_7$ (red) and $Tb_2Ti_2O_7$ (blue) (data points[39]). The presence of disordered magnetic moments in $Tb_2Ti_2O_7$ produces a strong scattering of phonons, seen as a massive suppression of κ_{xx} (15-fold at $T = 15$ K). **b**, Field dependence of κ_{xx}, plotted as $\Delta\kappa_{xx}(H)/\kappa_{xx}(0)$ versus H, with $\Delta\kappa_{xx} = \kappa_{xx}(H) - \kappa_{xx}(0)$, at $T = 15$ K (blue data points[12]). The strong effect of field (30% in 8 T) is a direct signature of the strong coupling between phonons and spins in $Tb_2Ti_2O_7$. Also shown is the transverse response in $Tb_2Ti_2O_7$ at $T = 15$ K, plotted as κ_{xy}/T versus H (red data points[12]). Note that in $Y_2Ti_2O_7$, $\kappa_{xy} = 0$ (ref. [12]). **c**, Thermal conductivity of two Nd-LSCO samples, on either side of p^* (red, $p = 0.24$; blue, $p = 0.21$), plotted as κ_{xx}/T versus T at $H = 18$ T (data points). We see that contrary to $Tb_2Ti_2O_7$ (**a**), the appearance of the negative κ_{xy} signal in Nd-LSCO below p^* is not accompanied by a large suppression of κ_{xx} (see Extended Data Fig. 3). **d**, Same as **b** but for LSCO $p = 0.06$, with the same x-axis and y-axis scales and data taken at (nearly) the same temperature (data points). We see that the situation in LSCO is very different to that found in $Tb_2Ti_2O_7$ (**b**): instead of having a small κ_{xy} and a large $\Delta\kappa_{xx}$ (**b**), we now have a large κ_{xy} and a small $\Delta\kappa_{xx}$. Quantitatively, $\kappa_{xy}/\Delta\kappa_{xx} \approx 1$ in LSCO and approximately 0.01 in $Tb_2Ti_2O_7$, at $T = 15$ K and $H = 8$ T (Table 1).

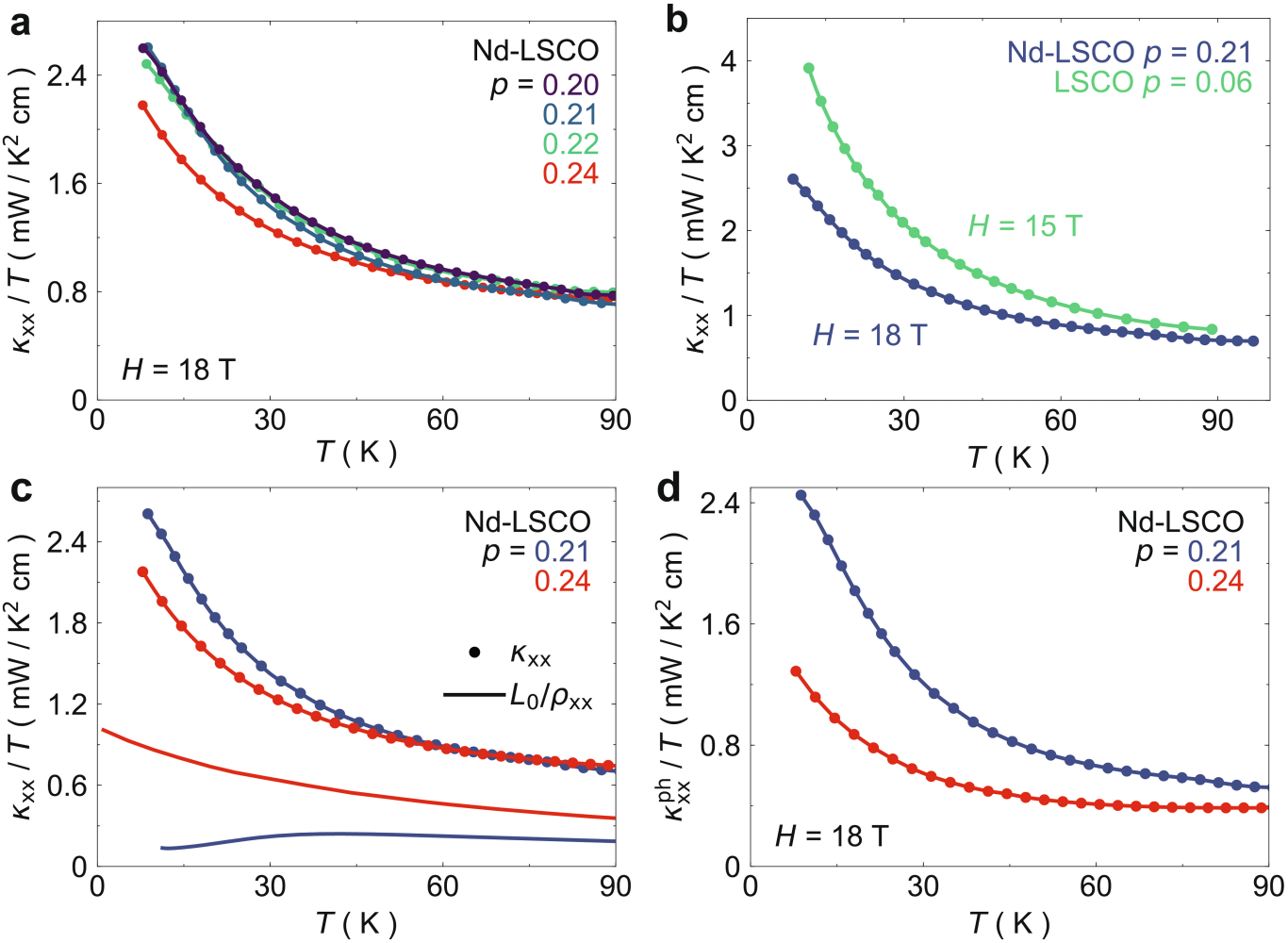

Extended Data Fig. 3 | Change in phonon κ_{xx} across p^* in Nd-LSCO. a, Thermal conductivity of Nd-LSCO at four different dopings, above p^* ($p = 0.24$) and below p^* ($p = 0.20, 0.21, 0.22$), plotted as κ_{xx}/T versus T, at $H = 18$ T (data points). We see that κ_{xx} increases below p^*. **b**, Same as **a** but for Nd-LSCO $p = 0.21$ (blue; $H = 18$ T) and LSCO $p = 0.06$ (green, $H = 16$ T). We see that κ_{xx} continues to increase as we lower p further. This shows that phonons conduct better at lower p. A natural explanation is that they are less scattered by charge carriers as the material becomes less metallic. **c**, Same data as in **a** for Nd-LSCO $p = 0.21$ (blue data points) and $p = 0.24$ (red data points), compared to the electrical conductivity of those same samples, plotted as L_0/ρ versus T (lines; measured at $H = 33$ T (ref. [17])). The latter curves are a reasonable estimate of the electronic thermal conductivity κ_{xx}^{el}, exact at $T \to 0$ (since the Wiedemann–Franz law is satisfied[40]), as seen in Fig. 2a. **d**, Estimate of the phonon conductivity, defined as $\kappa_{xx}^{ph} = \kappa_{xx} - L_0 T/\rho$, plotted as κ_{xx}^{ph}/T versus T (using data from **c**) (data points). We see that $\kappa_{xx}^{ph}(T)$ increases upon crossing below p^*, most probably because electron–phonon scattering is weakened by the loss of carrier density. There is no evidence that the phonons suddenly suffer from the onset of strong spin scattering below p^* (which would cause $\kappa_{xx}^{ph}(T)$ to drop below p^*), such as would be required to explain the appearance of the large negative κ_{xy} signal below p^* (Fig. 3) as being due to phonon transport.

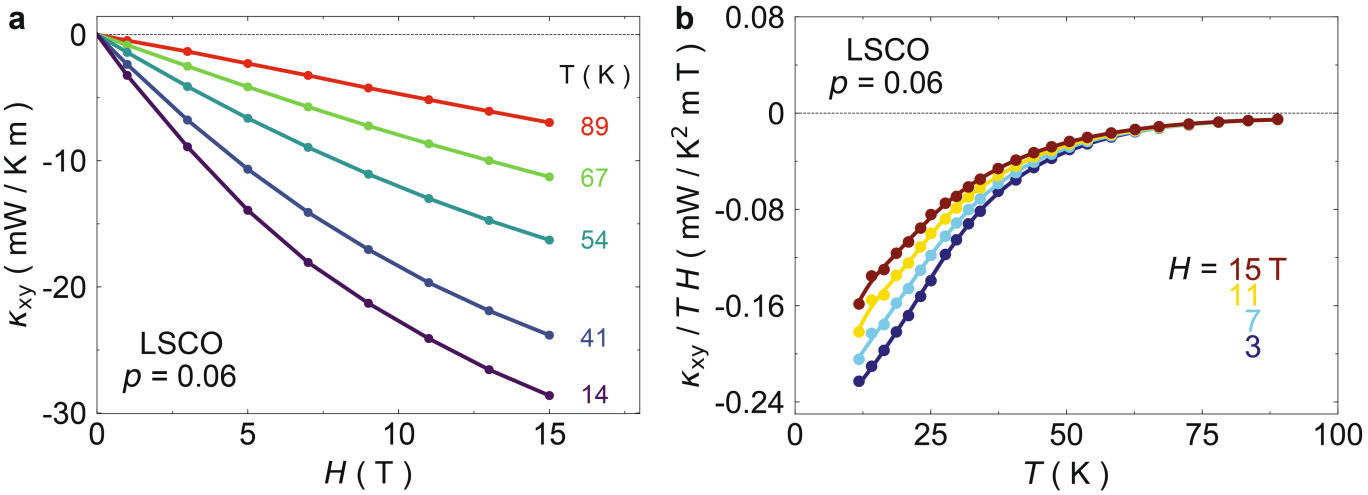

Extended Data Fig. 4 | Magnetic field dependence of κ_{xy} in LSCO. **a**, Field dependence of the thermal Hall conductivity of LSCO at $p = 0.06$, plotted as κ_{xy} versus H at various temperatures, as indicated (data points). The dependence of κ_{xy} on H is linear at high T and it becomes sublinear at lower T. **b**, Deviation from linearity displayed by plotting $\kappa_{xy}/(TH)$ versus T at four different fields H, as indicated (data points).

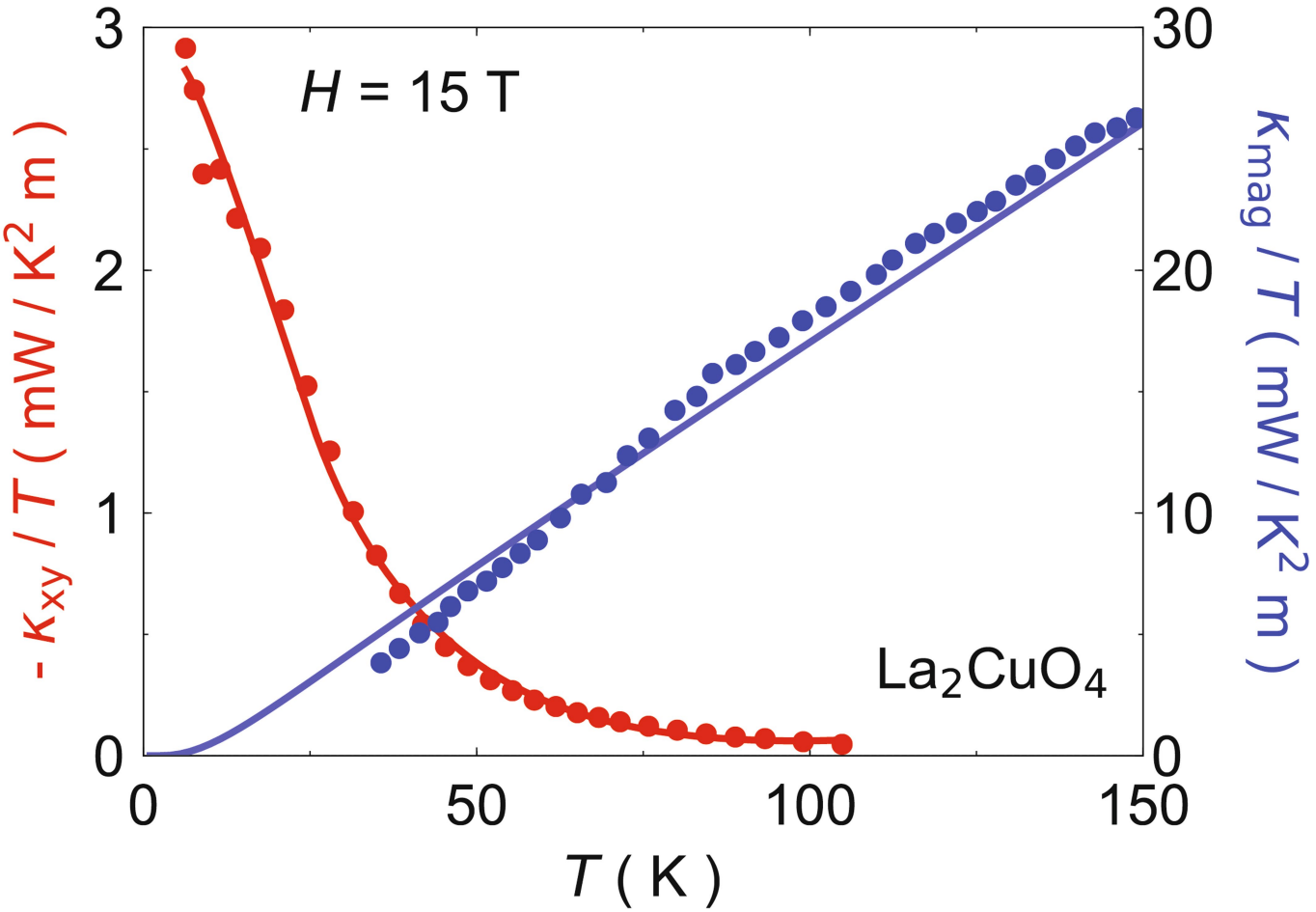

Extended Data Fig. 5 | Magnon thermal conductivity in La_2CuO_4. Thermal conductivity of magnons in La_2CuO_4, plotted as κ_{mag}/T versus T (blue data points, right axis; ref. [37]). The solid blue line is a fit to the data using the standard calculation for two magnon branches in 2D, with gaps as measured by neutron inelastic scattering[36], namely $\Delta_1 = 26$ K and $\Delta_2 = 58$ K. Below $T \approx 5$ K, thermally excited magnons are exponentially rare and $\kappa_{mag}/T \approx 0$. In sharp contrast, the thermal Hall conductivity of La_2CuO_4, $|\kappa_{xy}/T|$ (red data points, left axis; the red line is a guide to the eye; Fig. 1b), is largest at $T \approx 5$ K. This comparison shows that the κ_{xy} signal in La_2CuO_4 cannot come from magnon transport.

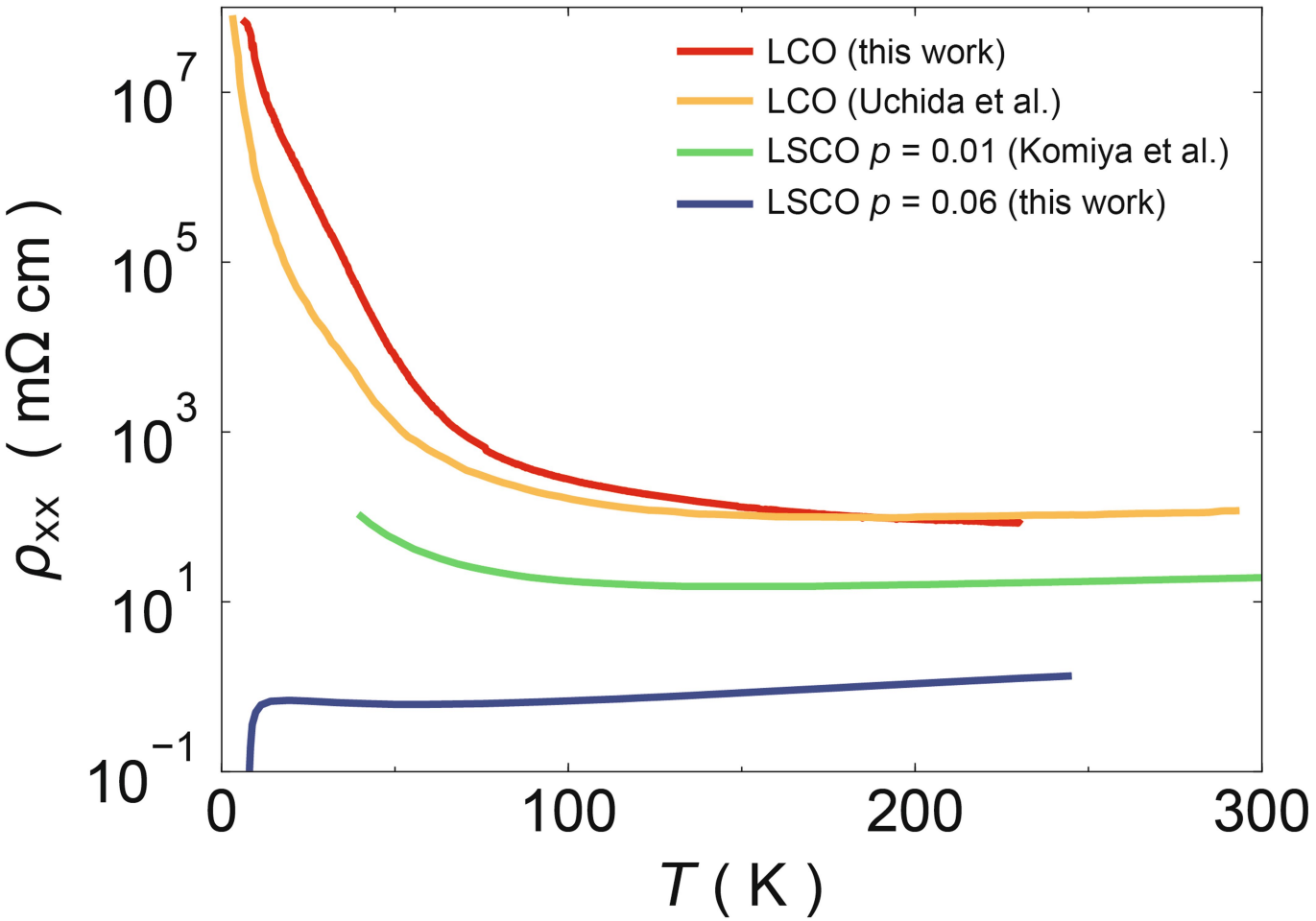

Extended Data Fig. 6 | Electrical resistivity in La_2CuO_4. Electrical resistivity, ρ_{xx}, of two of our samples—La_2CuO_4 (LCO, red) and LSCO at $p = 0.06$ (blue)—compared with published data for La_2CuO_4 (yellow[34]) and LSCO at $p = 0.01$ (green[35]). This shows that our LCO sample is very close to the Mott insulator La_2CuO_4, being more insulating than LSCO with $p = 0.01$ and much more insulating than our LSCO sample with $p = 0.06$.